Interaction between urban heat island and urban pollution island during summer in Berlin

Article *in* Science of The Total Environment · January 2018
DOI: 10.1016/j.scitotenv.2018.04.254

7 authors, including:

Huidong Li
Freie Universität Berlin
10 PUBLICATIONS **14** CITATIONS
SEE PROFILE

Tirthankar Chakraborty
Yale University
13 PUBLICATIONS **5** CITATIONS
SEE PROFILE

Sahar Sodoudi
Freie Universität Berlin
43 PUBLICATIONS **83** CITATIONS
SEE PROFILE

Science of the Total Environment 636 (2018) 818–828

Contents lists available at ScienceDirect

Science of the Total Environment

journal homepage: www.elsevier.com/locate/scitotenv

Interaction between urban heat island and urban pollution island during summer in Berlin

Huidong Li [a], Fred Meier [b], Xuhui Lee [c], Tirthankar Chakraborty [c], Junfeng Liu [d], Martijn Schaap [a,e], Sahar Sodoudi [a,*]

[a] Institute of Meteorology, Freie Universität Berlin, Berlin, Germany
[b] Institute of Ecology, Technische Universität Berlin, Berlin, Germany
[c] School of Forestry & Environmental Studies, Yale University, New Haven, USA
[d] College of Urban and Environmental Sciences, Peking University, Beijing, China
[e] Department Climate, Air and Sustainability, TNO, Utrecht, the Netherlands

HIGHLIGHTS

- Interaction between urban heat island and urban pollution island was studied.
- The impact of urban heat island on near-surface PM10 concentrations was investigated.
- The urban-rural differences in the incoming solar radiation and atmospheric longwave radiation were analyzed.
- The response of urban heat island to the urban-rural difference in absorbed radiation was quantified.

GRAPHICAL ABSTRACT

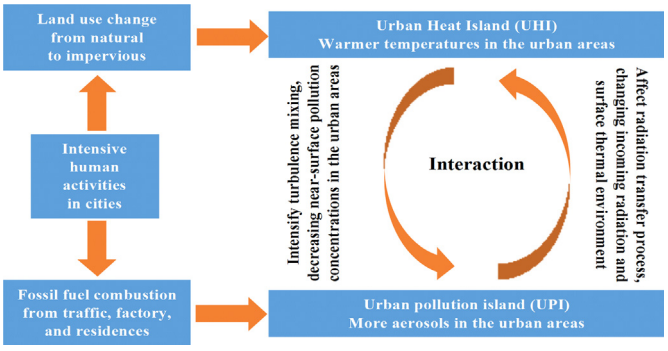

ARTICLE INFO

Article history:
Received 5 February 2018
Received in revised form 18 April 2018
Accepted 19 April 2018
Available online xxxx

Editor: SCOTT SHERIDAN

Keywords:
Urban Heat Island
Urban Pollution Island
Aerosol optical depth
Particulate matter
Urban-rural difference in radiation
Attribution method

ABSTRACT

Urban Heat Island (UHI) and Urban Pollution Island (UPI) are two major problems of the urban environment and have become more serious with rapid urbanization. Since UHI and UPI can interact with each other, these two issues should be studied concurrently for a better urban environment. This study investigated the interaction between the UHI and UPI in Berlin, through a combined analysis of in-situ and remote sensing observations of aerosols and meteorological variables in June, July, and August from 2010 to 2017. The atmospheric UHI (AUHI), surface UHI (SUHI), atmospheric UPI (AUPI), and near-surface UPI (NSUPI) were analyzed. The SUHI and AUPI are represented by the remote sensing land surface temperature (LST) and aerosol optical depth (AOD), and the AUHI and NSUPI are represented by the in-situ air temperature and Particulate Matter (PM10) concentrations. The study area shows spatial consistency between SUHI and AUPI, with higher LST and AOD in the urban areas. UHI strengthens the turbulent dispersion of particles in the urban areas, decreasing the NSUPI. The NSUPI intensity shows a negative relationship with the AUHI intensity, especially at night with a correlation coefficient of −0.31. The increased aerosols in urban atmosphere reduce the incoming solar radiation and increase the atmospheric longwave radiation in the urban areas. The response of the surface to the change of absorbed radiation is strong at night and weak during the day. This study estimates that the SUHI intensity is enhanced by around 12% at clear night by the increased absorbed radiation in the urban areas using an attribution method.

* Corresponding author.
E-mail address: sodoudi@zedat.fu-berlin.de (S. Sodoudi).

https://doi.org/10.1016/j.scitotenv.2018.04.254

The goal of this paper is to strengthen the understanding of the interactive influence between UHI and UPI and provide a basis for designing mitigation strategies of UHI and UPI.

1. Introduction

Intensive change of land use and emissions of air pollutants are two of the most important aspects of human activities in urban areas (McDonnell and MacGregor-Fors, 2016). The change of land surface from natural to impervious alters surface properties, resulting in lower albedo, higher Bowen ratio (ratio of sensible and latent heat flux), and larger energy storage of the surface in urban areas. As a result, urban areas produce warmer temperatures than the surrounding rural areas, which is called Urban Heat Island (UHI) phenomenon (e.g. Rizwan et al., 2008; Chakraborty et al., 2017). Meanwhile, the combustion of fossil fuels from factories, cars and other transportation means, as well as the daily human behaviour in cities emit a large number of pollution particles into the urban atmosphere (e.g. Ohara et al., 2007; Bonn et al., 2016). Thus, the urban atmosphere has more pollution particles than the rural atmosphere, which is called Urban Pollution Island (UPI) phenomenon (Crutzen, 2004). UHI increases the heat stress of city dwellers (e.g. Gabriel and Endlicher, 2011), while UPI increases the exposure of people to air pollutants (e.g. Monn and Becker, 1999; Han and Naeher, 2006). Furthermore, the superposition of heat stress and air pollution makes individuals more susceptible to the effect of each respective threat (e.g. Lai and Cheng, 2010; Meng et al., 2012; Burkart et al., 2013).

UHI and UPI can interact with each other. UHI-related warm temperatures can promote the dispersion of aerosol particles to higher atmospheric boundary level by increasing turbulent mixing (Sarrat et al., 2006). A temperature reduction in urban areas could decrease the rate of turbulent mixing and the height of mixing layer (Fallmann et al., 2016), leading to higher near-surface concentrations of PM10 (Fallmann, 2014). In turn, UPI-related increased aerosols in the urban atmosphere can generate larger radiative forcing. On the one hand, the increased aerosols can scatter more solar radiation back to space and reduce solar radiation reaching the urban surface (e.g. Jin et al., 2010; Wang et al., 2015). On the other hand, the increased aerosols can trap more earth-emitted infrared radiation and re-emit more longwave radiation to the urban surface (e.g. Lubin and Simpson, 1994; Cao et al., 2016). The UPI-induced larger radiative forcing in urban areas affects the urban thermal environment and changes the UHI. Cao et al. (2016) reported that the haze in semi-arid Chinese cities enhanced the surface UHI intensity by 0.7 K at night.

Considering the interaction of UHI and UPI is important for a comprehensive understanding of the urban environment. However, most of the previous studies on UHI and UPI were conducted separately. Insufficient knowledge of the interaction between UHI and UPI inhibits the development of integrative mitigation strategies. Nowadays, fast urbanization process further strengthens UHI and UPI (e.g. Wei and Ye, 2014; AAAS, 2016). The interactive impacts of growing UHI and UPI are becoming a new direction for future studies (Crutzen, 2004). Baklanov et al. (2016) reviewed the previous studies on the complex interactions between climate, air quality, and megacities, and addressed the importance of the integrated studies of urban climate and air pollution in the changing climate. Recent European project MEGAPOLI focused on the feedbacks and interlinkages between climate change and regional air quality related to megacities (Baklanov et al., 2010). In China, the study of the interaction between air pollution and the physical state of the atmospheric boundary layer was taken as a priority study area of boundary layer meteorology (Lee et al., 2015). The modelling of urban air pollution and climate interactions was widely discussed in the 9th International Conference in Air Quality - Science and Application (Sokhi et al., 2017).

In this study, we attempted to connect UHI and UPI and carried out an integrated study of these two problems in the city of Berlin, Germany. In-situ and remote sensing observations of aerosols and meteorological variables in June, July, and August from 2010 to 2017 were collected. The atmospheric UPI (AUPI), near-surface UPI (NSUPI), atmospheric UHI (AUHI), and surface UHI (SUHI) were analyzed. The AUPI describes the urban-rural difference of the aerosol optical depth (AOD) from remote sensing observation, and the NSUPI describes the urban-rural difference of the near-surface aerosol concentrations characterized by the in-situ observation of Particulate Matter (PM10). The AUHI describes the urban-rural difference of the air temperature from in-situ observation, and the SUHI describes the urban-rural difference of the land surface temperature (LST) from remote sensing observation. The study consists of three sections. Firstly, the relationship between the SUHI and AUPI in spatial variations was investigated using remote sensing data. Secondly, the impact of the AUHI on the NSUPI was examined using in-situ observations. Thirdly, the impact of the AUPI on the radiation transfer was studied by comparing the incoming solar radiation and atmospheric longwave radiation between the urban and rural areas. Moreover, the response of the SUHI to the urban-rural difference of the absorbed radiation was analyzed using an attribution method (Cao et al., 2016). Given the strong UHI (Fenner et al., 2014) and the good quality of remote sensing observation under cloudless conditions in the summer of Berlin (Li et al., 2018), this study only focuses on the summer period in June, July, and August. The goal of this study is to improve the understanding of the interactive influence between urban thermal environment and air pollution, and provide a scientific basis for the mitigation of these two problems.

2. Study area, datasets, and methodology

2.1. Study area

The study area is Berlin, the capital city of Germany. Berlin (52.34°–52.68° N, 13.10°–13.77° E) is located in Northeastern Germany and covers an area of around 900 km^2. Berlin has a temperate maritime climate with the annual mean temperature of 9.5 °C and annual precipitation of 591 mm. Affected by the prevailing westerlies, the wind mainly comes from the west directions in summer (Fig. S1). Berlin has >3.6 million inhabitants, with one-third living in the inner city. Based on Corine land cover datasets (Feranec et al., 2007), around 35% of the area is covered by buildings, and around 20% of the area is covered by transportation/infrastructure in Berlin (Fig. 1a). Most of the non-urban area is covered by forest and farmland. The large built-up area creates distinct AUHI (e.g. Fenner et al., 2014; Li et al., 2017) and SUHI in this city (e.g. Li et al., 2017, 2018). The UHI-enhanced heat wave has a negative impact on the health of the Berlin dweller (Gabriel and Endlicher, 2011; Scherer et al., 2014). Meanwhile, Berlin suffers from air pollution. The air quality cannot meet the standards of the European Union in terms of PM10 (Görgen and Lambrecht, 2007). The local emissions are the dominant source of the elevated urban particulate number and mass concentrations (Bonn et al., 2016). The fine mode aerosols are the dominant component of PM10, accounting for around three-quarters of the observed PM10 mass. Road traffic is the major emission source, due to a large number of vehicles (Lutz, 2013) and a dense traffic network in Berlin (Fig. 1.b). In 2015, 1.37 million motor vehicles were registered in the city (389 cars per 1000 residents). The traffic intensity is high in the urban center and low in the rural areas. The urban-rural differences in the emissions and air pollutants are significant (Kuik et al., 2016).

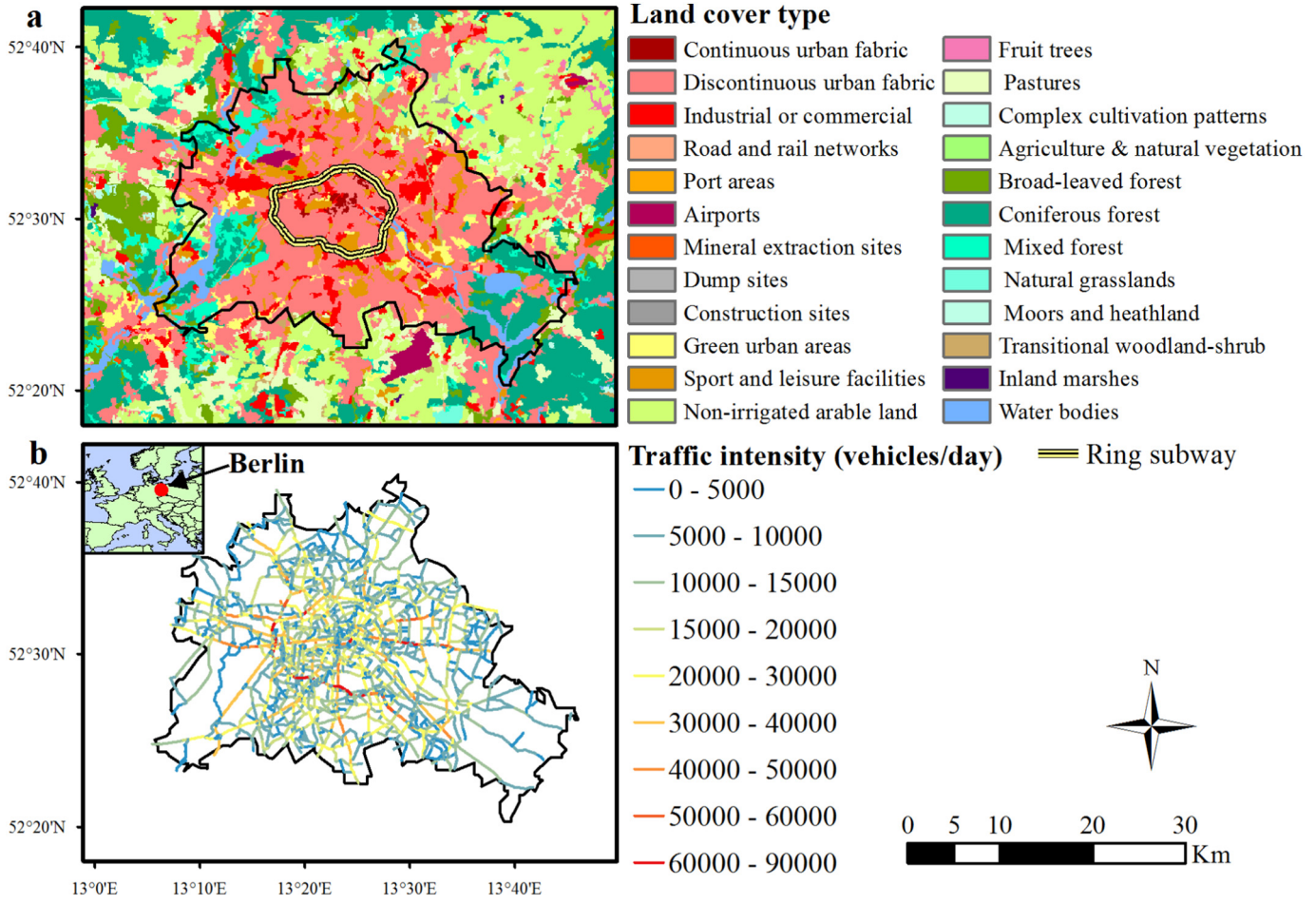

Fig. 1. Spatial patterns of the (a) land cover and (b) traffic intensity in the study area. The land cover data in (a) are Corine land cover data version 2012. The traffic intensity map in (b) is the average daily traffic volume version 2014, which comes from the FIS Broker of the Senate Department for Urban Development and the Environment, Berlin.

2.2. Datasets and processing

2.2.1. Remote sensing AOD and LST

Moderate Resolution Imaging Spectroradiometer (MODIS) observed AOD product (MYD04_3K) at a 3000 m resolution and LST product (MYD11_A1) at a 1000 m resolution (collection 006) by Aqua satellite were used in this study. The Aqua satellite passed over the city of Berlin at UTC time around 11:50 in the daytime and 1:20 at night. MYD04_3K AOD data are derived from dark target algorithms at 550 nm (Munchak et al., 2013; Remer et al., 2013). The AOD data with the best quality (Flag = 3) were used in this study. Comparison of the MODIS AOD against sun photometer observations at station of Free University of Berlin shows a good agreement, with a correlation coefficient of 0.90 ($p < 0.01$) and a RMSE of 0.05 (Fig. S2). MYD11_A1 LST data were retrieved using the generalized split-window algorithm (Wan and Dozier, 1996). The retrieval of LST was further refined by correcting bias resulting from cloud contamination and topographic differences (Wan, 2008). The collection 6 LST data achieve reliable quality with the standard deviation of errors <0.5 K (Wan, 2014). The AOD and LST data from 2010 to 2017 in June, July, and August were downloaded from the NASA website. In order to investigate the relationship of the spatial configurations of the AOD and LST, the LST data were re-projected to 3000 m resolution grids using the online post-processing tool on the NASA website. The post-processing tool supports the following operations: subset by dataset name, subset by geographic area of interest or shape, gridding swath data, reprojection to new map projection, mosaic, and reformat to different file formats. The detailed introduction of the online tool refers to https://ladsweb.modaps.eosdis.nasa.gov/tools-and-services/. The mean spatial patterns of AOD and LST were calculated using the images with more than three quarters of grids cloud free.

2.2.2. In-situ observations of PM10, air temperature, radiation, cloud, and wind

In-situ observed PM10, air temperature, incoming radiation, clouds, and wind speed were used in this study (Table 1). Hourly near-surface PM10 concentrations data from 2010 to 2015 were collected at twelve stations. Three rural background stations are located in the rural near-city areas that are far away from anthropogenic emissions, three urban background stations are located in the urban areas that are influenced by the local anthropogenic emissions, but are far away from traffic emission sources, and six traffic stations are located on the urban areas close to traffic emissions. Detailed information about the PM10 observation stations refers to the study of Shahraiyni et al. (2015). Hourly 2 m air temperature data from 2010 to 2015 were collected at four stations (Potsdam, Schoenefeld, Tempelhof, and Fasanenstrasse). Hourly incoming solar radiation data were collected at seven stations (FUB, Tegel, TUB, Wiener, HTW, Potsdam, and Lindenberg), and hourly incoming atmospheric longwave radiation data were collected at four stations (TUB, Wiener, Potsdam, and Lindenberg). The stations FUB, Tegel, TUB, Wienerstrasse, and HTW are located in the urban areas, while the stations Potsdam and Lindenberg are located in the near-city and far-city rural areas, respectively. Hourly cloud cover data were collected at two urban stations (Tegel and Dahlem) and two rural stations (Potsdam and Lindenberg). Hourly wind speed data were collected at Potsdam station. Summer (June, July, and August)

Table 1
The geographic information, operator, land cover, and time series of the in-situ observation data.

Variables	Stations	Operator*	Lon (E)	Lat (N)	Urban/rural	Corine land cover	Time series
PM10	Grunewald	BLM	13.23	52.47	Rural background	Coniferous forest	2010–2015
	Buch	BLM	13.49	52.64	Rural background	Industrial or commercial	2010–2015
	Friedrichshagen	BLM	13.65	52.45	Rural background	Industrial or commercial	2010–2015
	Wedding	BLM	13.35	52.54	Urban background	Industrial or commercial	2010–2015
	Nansenstr	BLM	13.43	52.49	Urban background	Industrial or commercial	2010–2015
	Mitte	BLM	13.42	52.51	Urban background	Industrial or commercial	2010–2015
	Hardenbergplatz	BLM	13.33	52.51	Urban Traffic	Continuous urban fabric	2010–2013
	Steglitz	BLM	13.32	52.46	Urban Traffic	Industrial or commercial	2010–2015
	Mariendorf	BLM	13.39	52.44	Urban Traffic	Industrial or commercial	2010–2015
	Silbersteinstr	BLM	13.44	52.47	Urban Traffic	Industrial or commercial	2010–2015
	Friedrichshain	BLM	13.47	52.51	Urban Traffic	Industrial or commercial	2010–2015
	Karl-Marx-Str	BLM	13.43	52.48	Urban Traffic	Industrial or commercial	2010–2015
Radiation	FUB	FU	13.31	52.46	Urban	Discontinuous urban fabric	2010–2015
	Tegel	DWD	13.31	52.46	Urban	Airports	2016–2017
	HTW	HTW	13.52	52.46	Urban	Industrial or commercial	2017
	TUB	TU	13.33	52.51	Urban	Industrial or commercial	2014–2017
	Wiener	TU	13.43	52.50	Urban	Discontinuous urban fabric	2014–2017
	Potsdam	DWD	13.06	52.38	Rural	Green urban areas	2010–2017
	Lindenberg	DWD	14.12	52.21	Rural	Discontinuous urban fabric	2010–2017
Cloud	Dahlem	FU	13.31	52.46	Urban	Industrial or commercial	2010–2017
	Tegel	Same as Tegel above					2010–2017
	Potsdam	Same as Potsdam above					2010–2017
	Lindenberg	Same as Lindenberg above					2010–2017
Air temperature	Fasanenstrasse	FU	13.34	52.51	Urban	Industrial or commercial	2010–2017
	Tempelhof	DWD	13.40	52.47	Urban	Sport and leisure facilities	2010–2017
	Schoenefeld	DWD	13.53	52.38	Rural	Airports	2010–2017
	Potsdam	Same as Potsdam above					2010–2017
Wind	Potsdam	Same as Potsdam above					2010–2017

*BLM = Berliner Luftgüte Messnetz, http://www.berlin.de/senuvk/umwelt/luftqualitaet/luftdaten/index.shtml; FU = Freie Universität Berlin, http://www.geo.fu-berlin.de/en/met/service/stadtmessnetz/index.html; DWD = Deutscher Wetterdienst, German Weather Service, www.dwd.de; HTW = Hochschule für Technik und Wirtschaft, http://wetter.htw-berlin.de/; TU = Technische Universität Berlin, https://www.klima.tu-berlin.de/index.php?show=forschung_dch_messnetz&lan=en.

observations were used in this study. The analysis was conducted for day and night, respectively. The daytime (5:00–21:00 CET) period and nighttime (22:00–4:00 CET) period were defined as the hours with and without solar radiation at Potsdam station, respectively. The geographic information of the stations and the time series of the observation data are listed in Table 1.

2.3. Methodology

2.3.1. Calculations of the intensities of AUHI and SUHI

The intensities of SUHI and AUHI quantify the urban-rural difference of the land surface temperature and air temperature, respectively. In this study, the former was calculated using remote sensing observations, and the latter was calculated using in-situ observations. The SUHI intensity was calculated as the difference of the mean MODIS LST of the urban grids within the ring subway and of the rural grids outside the border of Berlin (Fig. 1a), which were selected using the shapefiles of the ring subway and the city border through Matlab. The AUHI intensity was calculated as the difference of the mean air temperature at two urban stations (Fasanenstrasse and Tempelhof) and at two rural stations (Potsdam and Schoenefeld). Given the influence of strong wind to the advective transport of heat, the AUHI observed under wind speed faster than 3 m/s was omitted for analysis.

2.3.2. Calculations of the intensities of AUPI and NSUPI

The intensities of AUPI and NSUPI quantify the urban-rural difference of the AOD and near-surface PM10, respectively. In this study, the former was calculated using remote sensing observations, and the latter was calculated using in-situ observations. The AUPI intensity was calculated as the difference of mean MODIS AOD of the urban grids within the ring subway and of the rural grids outside the border of Berlin (Fig. 1a), which were selected using the shapefiles of the ring subway and the city border through Matlab. The NSUPI intensity was calculated as the difference of the mean PM10 at urban stations and at rural stations. The urban areas have urban background stations and traffic stations. The NSUPI intensity calculated using urban background station data was defined as NSUPI_B intensity, while the NSUPI intensity calculated using traffic station data was defined as NSUPI_T intensity. The NSUPI_B intensity reflects the integrated influence of anthropogenic emissions on the near-surface PM10 concentrations, while the NSUPI_T reflects the strong impact of traffic emissions. Given the influence of strong wind to the advective transport of aerosol particles, the NSUPI observed under strong wind conditions with speed >3 m/s was omitted for analysis.

2.3.3. Calculation of the change of SUHI intensity caused by the urban-rural difference of incoming radiation

The change of SUHI intensity caused by the urban-rural difference of incoming radiation was calculated using an attribution method. The attribution method was developed to investigate the mechanism that caused the change of surface temperature by Lee et al. (2011). Zhao et al. (2014) further developed this method for SUHI studies, and investigated the attributions that caused SUHI for cities across North America. Cao et al. (2016) studied the impact of haze on SUHI intensity in China using this method. The incoming radiations in urban and rural areas usually show difference due to UPI-related different loading aerosols, which has an impact on the UHI. The physical mechanisms of the impact of UPI on the radiation and UHI were discussed in Sections 4.2 and 4.3. Referring to the study of Cao et al. (2016), the change of SUHI intensity ($\Delta SUHII$, K) caused by the urban-rural difference of incoming radiation was calculated as.

$$\Delta SUHII = \frac{\lambda_0}{1+f}[(1-\alpha_u)S_u-(1-\alpha_r)S_r+L_u-L_r] \quad (1)$$

where S_u and S_r, and L_u and L_r are the incoming solar radiation and atmospheric longwave radiation in the urban and rural areas, respectively. α_u and α_r are the surface albedo of urban and rural areas. λ_0 is the local

climate sensitivity ($\lambda_0 = 1/4\sigma T_s^3$), and f is energy redistribution factor and is defined as.

$$f = \frac{\rho C_p}{4 r_a \sigma T_s^3}\left(1 + \frac{1}{\beta}\right) \quad (2)$$

where T_s is surface temperature; σ is Stephan Boltzmann constant, 5.67×10^{-8} W/(m^2 K^4); C_p is the specific heat of air at constant pressure, 1004 J/(Kg K); ρ is air density; r_a is aerodynamic resistance to heat diffusion; β is Bowen ratio.

In this study, the radiation data come from in-situ observations at urban and rural stations (Table 1). The radiation data were filtered under clear-sky conditions that the cloud fraction at all stations was less than or equal to 2 oktas and the cloud fraction at the rural stations was equal to or larger than that at the urban stations. In order to eliminate the impact of small clouds on the radiation observations, the radiation data with the urban-rural difference outside 5% and 95% at each hour were omitted for the calculation of hourly mean values. The values of α_u and α_r were calculated using MODIS Albedo 16-Day L3 Global product (MCD43C3) collection 6 at a 0.05 degree resolution (Schaaf et al., 2002). MODIS Albedo data from 2014 to 2017 in summer (June, July, and August) were used. MODIS albedo was compiled based on the bidirectional reflectance distribution function (BRDF) and includes Black-sky (α_{bsa}) and White-sky (α_{wsa}) albedo. The integrated albedo was calculated as.

$$\alpha = (1-bw)\alpha_{bsa} + bw\alpha_{wsa} \quad (3)$$

where bw is the ratio of diffuse solar radiation to direct solar radiation. The value of bw (0.27) was calculated using the observed diffuse and global solar radiation under clear-sky conditions in June, July, and August during 2014–2017 at Potsdam station. The mean albedo over urban (0.12) and rural (0.14) areas were calculated using the albedo within the ring subway and outside the border of Berlin, respectively, consistent with the calculation of SUHI intensity (Fig. S3). The values of λ_0 and f were calculated using MERRA 2 reanalysis data (Gelaro et al., 2017) in June, July, and August during 2014–2017. Referring to the study of Zhao et al. (2014), the r_a was calculated as.

$$r_a = \frac{\rho C_p (T_S - T_a)}{SH} \quad (4)$$

and the β was calculated as.

$$\beta = SH/LH \quad (5)$$

where T_a is air temperature. SH and LH are sensible heat flux and latent heat flux. The calculations of r_a and β were performed for the whole day, with rainy and cloudy hours omitted. The values of ρ, T_s, T_a, SH, LH, precipitation, and cloud come from MERRA 2 reanalysis data at the grid that Berlin is located. In order to eliminate the outliers, the resulted r_a, β, and f outside 5% and 95% were omitted for the calculation of hourly mean values. The calculation and statistical work were conducted using Matlab.

3. Results

3.1. Relationship between the SUHI and AUPI in spatial variations

The relationship between the SUHI and AUPI in spatial variations was analyzed using MODIS LST and AOD. High AOD values are mainly located in the central city within the ring subway (Fig. 2). The AOD in the surrounding rural areas is much lower than that in the urban areas. The study areas show a AUPI, with the intensity of 0.08. Meanwhile, the urban stations show higher PM10 concentrations than the rural stations. The spatial pattern of the PM10 concentrations is consistent with that of the AOD. The city is clearly a source of aerosols, due to the combined human activities, especially the traffic, which is the major emission source. Hence, the traffic stations show the highest PM10 concentrations. Besides, the spatial variation of aerosols is affected by wind. There is a plume in the downwind areas in the eastern Berlin, due to the prevailing westerly wind in summer (Fig. S1). Berlin also shows significant SUHI, with higher LST in the urban areas than in the rural areas (Fig. 3). The SUHI intensities are 5.38 and 2.84 K for the daytime and nighttime, respectively. The SUHII during the day is higher than that at night, which is consistent with the previous studies (e.g. Schwarz et al., 2011; Li et al., 2017). The spatial patterns of the SUHI are similar with that of the AUPI. Generally, the LST shows a positive correlation with the AOD in spatial variations. This phenomenon is consistent with the study in other cities (Xu et al., 2013). The correlation coefficient between the LST and AOD is 0.62 ($p < 0.01$) during the day.

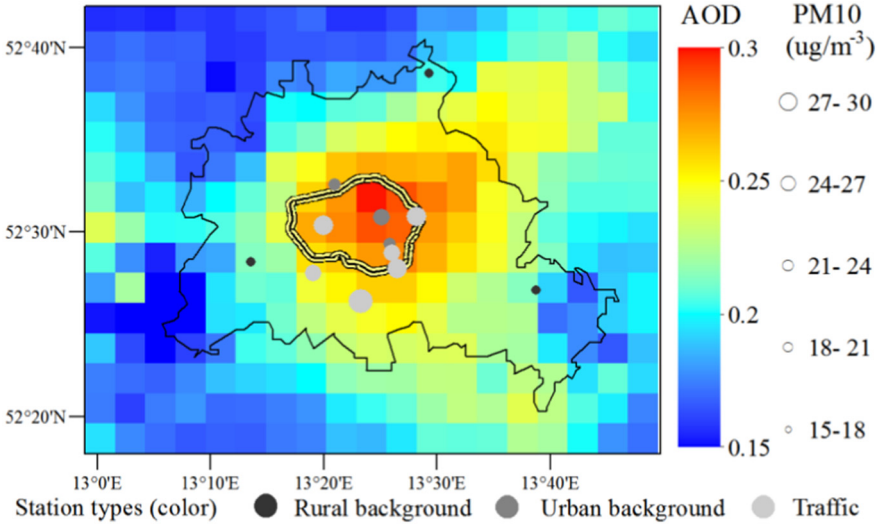

Fig. 2. Spatial patterns of the mean AOD and PM10 in July, July, and August from 2010 to 2017. The color and size of the circles show the types of the observation stations and the values of the observed PM 10 concentrations, respectively. The mean AOD were calculated using the images with more than three quarters of grids cloud free and the mean PM10 were calculated using the observations under wind speed <3 m/s.

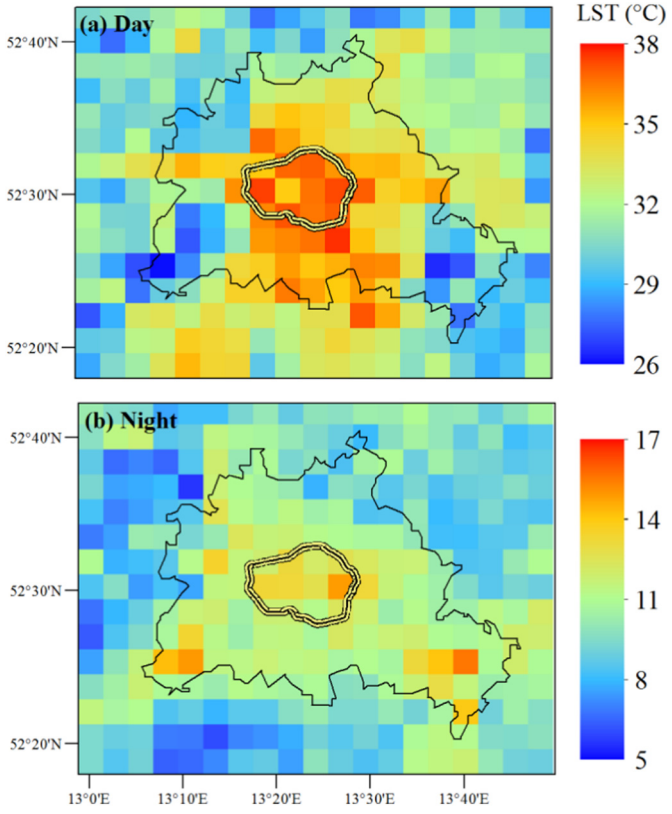

Fig. 3. Spatial patterns of the mean LST (a) during the day and (b) at night in June, July, and August from 2010 to 2017. The mean LST were calculated using the images with more than three quarters of grids cloud free.

3.2. The influence of AUHI on NSUPI

The diurnal variations of the mean PM10 concentrations of three types of observation stations were compared (Fig. 4). The diurnal variation of the PM10 concentrations of the rural background stations shows larger values at night and smaller values during the day. Atmospheric turbulence controls the aerosol concentrations at the rural background stations. Strong turbulent mixing during the day boosts the dispersion of aerosol particles and vice versa at night. The PM10 concentrations

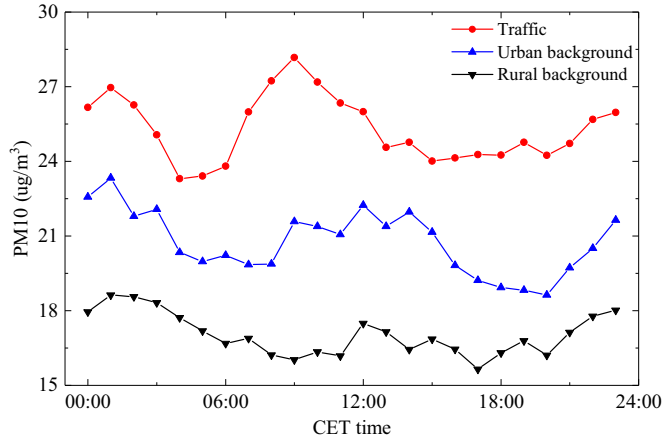

Fig. 4. Diurnal variations of the mean PM10 observed at traffic stations (red), urban background stations (blue), and rural background stations (black) in June, July, and August from 2010 to 2015. The mean PM10 were calculated using the observations under wind speed <3 m/s. (For interpretation of the references to color in this figure legend, the reader is referred to the web version of this article.)

at the urban background stations and traffic stations are jointly controlled by turbulent mixing and anthropogenic emissions. At the urban background stations, turbulent mixing plays a dominant role in the PM10 concentrations, with smaller values in the daytime than in the nighttime. But there are several peaks during the day, due to the effect of emissions. At the traffic stations, emissions from intensive vehicles play a dominant role in the aerosol concentrations. Especially during the heavy traffic period in the morning, the PM10 concentrations of the traffic stations reach peak values. The influence of the anthropogenic emissions on the aerosol concentrations mainly happens during the day. Generally, the difference of the mean PM10 concentrations among the three types of stations is larger in the daytime than in the nighttime.

UHI-related warm temperatures could decrease aerosol concentrations in urban areas and NSUPI by strengthening turbulent mixing. The NSUPI intensity shows a negative correlation with the AUHI intensity for both daytime and nighttime (Fig. 5). The NSUPI intensity decreases with the increase in the AUHI intensity. The correlation coefficients between NSUPI_B intensity and NSUPI_T intensity and AUHI intensity are −0.17 and −0.15 ($p < 0.01$) during the day, and −0.31 and −0.30 ($p < 0.01$) at night. The impact of the anthropogenic emissions on the NSUPI was not excluded from the correlation analysis in Fig. 5. Therefore, the correlation coefficients are not high. The nighttime shows a better NSUPI-AUHI relationship due to the less disturbance from anthropogenic emissions, as most of the anthropogenic emissions stop at night. Moreover, the relationship between NSUPI_B intensity and AUHI intensity is slightly better than the relationship between NSUPI_T intensity and AUHI intensity, because the urban background stations are less affected by traffic emissions.

3.3. Comparison of the incoming solar radiation and atmospheric longwave radiation between urban and rural areas

Increased aerosols in urban areas affect the radiation transfer process. Under the clear sky conditions, urban stations show lower solar radiation and higher atmospheric longwave radiation than the rural stations Potsdam (Fig. 6a) and Lindenberg (Fig. 6b). The urban-rural differences reach −30.07 and − 48.06 W/m^2 for the solar radiation, and 13.26 and 20.38 W/m^2 for the atmospheric longwave radiation in the midday, respectively (Fig. 6c and d). The difference between urban stations and Lindenberg station is larger than the difference between urban stations and Potsdam station because the Lindenberg station is less affected by anthropogenic emissions due to its longer distance to urban areas than the Potsdam station. The decrease of the incoming solar radiation in urban areas is larger than the increase of the atmospheric longwave radiation. However, the absorption of solar radiation by the ground is affected by the surface albedo. The urban areas with lower albedo can absorb solar radiation more efficiently than the rural areas. The urban-rural difference of the absorbed solar radiation becomes much smaller than the urban-rural difference of incoming solar radiation (Fig. 6e and f) and is even smaller than the urban-rural difference of the atmospheric longwave radiation sometimes. As a result, the urban-rural differences of the net absorption of radiation, $(1-\alpha_u)S_u-(1-\alpha_r)S_r + L_u-L_r$, become rather small and even positive at some hours during the day (Fig. 6e and f).

3.4. The ΔSUHII caused by the urban-rural difference of net absorption of radiation

The urban-rural difference of the net absorption of radiation can affect the SUHI. Based on Eq. (1), the sensitivity of the surface to the change of net absorption of radiation is controlled by $\lambda_0/(1 + f)$. The λ_0 has a small daily range from 0.16 to 0.19 (K m^2)/W (Fig. 7a). The f is the dominant factor of the surface sensitivity. The f shows a significant diurnal variation, with large values during the day, while low values at night (Fig. 7b). The values of f are mainly determined by the aerodynamic

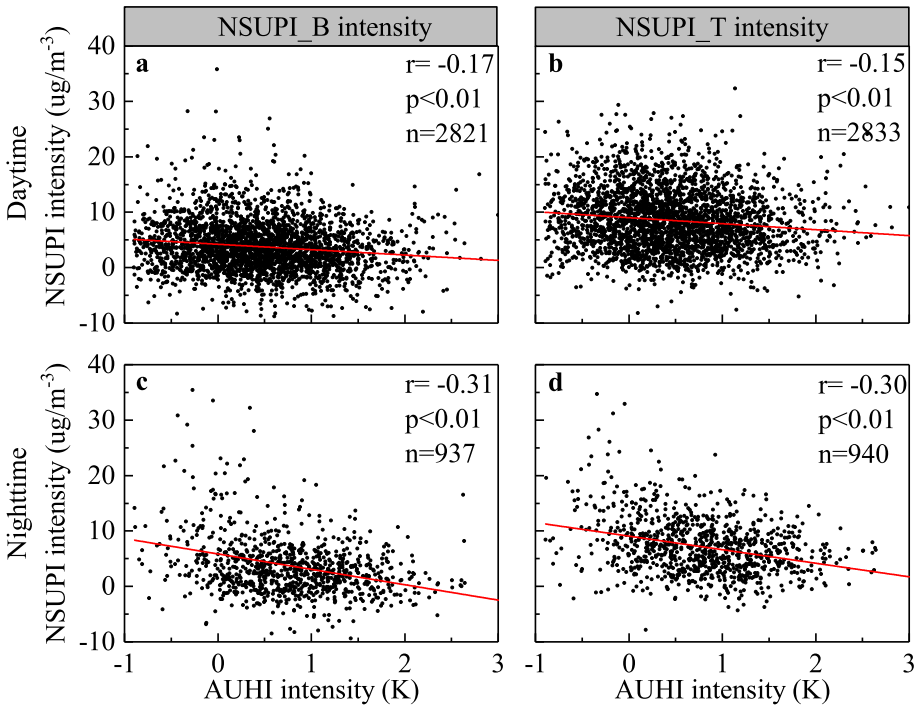

Fig. 5. Scatter plots of the NSUPI intensity and AUHI intensity for daytime (upper panels) and nighttime (lower panels) in June, July, and August from 2010 to 2015. Subplots (a) and (c) show NSUPI_B intensity, while subplots (b) and (d) show NSUPI_T intensity. The PM10 data observed under wind speed <3 m/s were shown here.

resistance and Bowen ratio. During the day, the low aerodynamic resistance produced high *f*, while at night, the high aerodynamic resistance and the negative Bowen ratio produced low *f* (Fig. S4). Especially in the evening from 18:00 to 21:00 CET, the values of *f* change drastically, because of the transition of negative and positive Bowen ratio with small absolute values. The calculated *f* during this period was omitted for the following analysis. At night, the values of *f* are around 2.06, which are between the values of humid and semi-humid zones of China (Cao et al., 2016). The daily mean *f* is 7.80, similar to the study of Bright et al. (2017) in the same latitude. The $\lambda_0/(1+f)$ shows large values at night and low values during the day (Fig. 7c). Affected by the drastic change of *f*, the $\lambda_0/(1+f)$ shows extreme values in the evening.

The diurnal variation of the calculated ΔSUHII is presented in Fig. 8. Given the extreme values of $\lambda_0/(1+f)$ from 18:00 to 21:00 CET could lead to unreasonable ΔSUHII, the calculation results during this period are not shown here and are excluded for the calculation of mean values. The ΔSUHII shows positive values at night. The mean values of $\Delta SUHII_{Potsdam}$ and $\Delta SUHII_{Lindenberg}$ are 0.33 ± 0.09 and 0.40 ± 0.09 K, respectively (Table 2). Potsdam station is located in the rural areas, which are selected for the calculation of SUHI intensity. The mean $\Delta SUHII_{Potsdam}$ accounts for 12 ± 3% of the nighttime SUHI intensity in Fig. 3b. The SUHI intensity is enhanced at night, consistent with the study of Cao et al. (2016). The daytime ΔSUHII is rather minor, with mean values of 0.06 ± 0.07 and 0.00 ± 0.13 K for the $\Delta SUHII_{Potsdam}$ and $\Delta SUHII_{Lindenberg}$, respectively, because of the offset of the absorbed solar radiation and longwave radiation (Fig. 6e and f) and low $\lambda_0/(1+f)$ during the day (Fig. 7c). Compared to the high daytime SUHI intensity, the daytime ΔSUHII is negligible.

4. Discussion

4.1. The mechanism for the impact of UHI on NSUPI

Atmospheric turbulence plays a dominant role in the upward transport of aerosol particles in the atmospheric boundary layer (Sarrat et al., 2006). Wagner and Schäfer (2017) reported a strong correlation between pollution concentrations and boundary layer height. UHI-related warm temperatures in urban areas strengthen turbulent mixing and increase the height of urban boundary layer (e.g. Dupont et al., 1999; Fallmann et al., 2016). Sarrat et al. (2006) found that the urban boundary layer was two to three times higher than the rural one over Paris. Epstein et al. (2017) found that the urban boundary layer height decreased by 60% with AUHI intensity decreased by 0.35 K. Strong turbulence boosts the dispersion of aerosol particles inside a deeper boundary layer, decreasing the aerosol concentrations in urban areas and weakening the NSUPI intensity. At night, the particles in the rural atmosphere are usually trapped in a near-surface layer, due to the temperature inversion (Oke, 1995). While there is still a mixing layer below temperature inversion in the urban atmosphere, due to the release of the stored energy in the urban surface (Godowitch et al., 1985; Gedzelman et al., 2003). The turbulent mixing can weaken the accumulation of aerosol particles in the near-surface level at night, decreasing the nighttime near-surface aerosol concentrations in urban areas. Rendón et al. (2014) reported that urbanization could break up temperature inversion, improving air quality.

However, it should be noted that our results about AUHI-NSUPI relationship are achieved using the data observed in summer, when the atmosphere is unstable and the turbulent mixing is strong. In winter, the atmosphere is relatively stable with weak turbulence. The relationship between AUHI on NSUPI may become weak then, because of the small urban-rural difference of the intensity of turbulent mixing and of the height of atmospheric boundary layer. Meanwhile, it should be noted that the NSUPI is jointly affected by anthropogenic emissions and UHI. The correlation analysis between NSUPI and UHI intensity in this study did not exclude the impact of emissions, resulting in the low correlation coefficients, especially during the day (Fig. 5). All these problems need further studies in the future. Additionally, this study defined NSUPI using PM10 data. Besides PM10, other indicators, such as TSP, also can represent the characteristic of aerosol concentrations and can be used to define NSUPI. The definition of NSUPI needs further study.

4.2. The mechanism for the urban-rural difference of incoming radiation

Atmospheric aerosols can affect both the incoming solar radiation and atmospheric longwave radiation on the surface (Haywood and

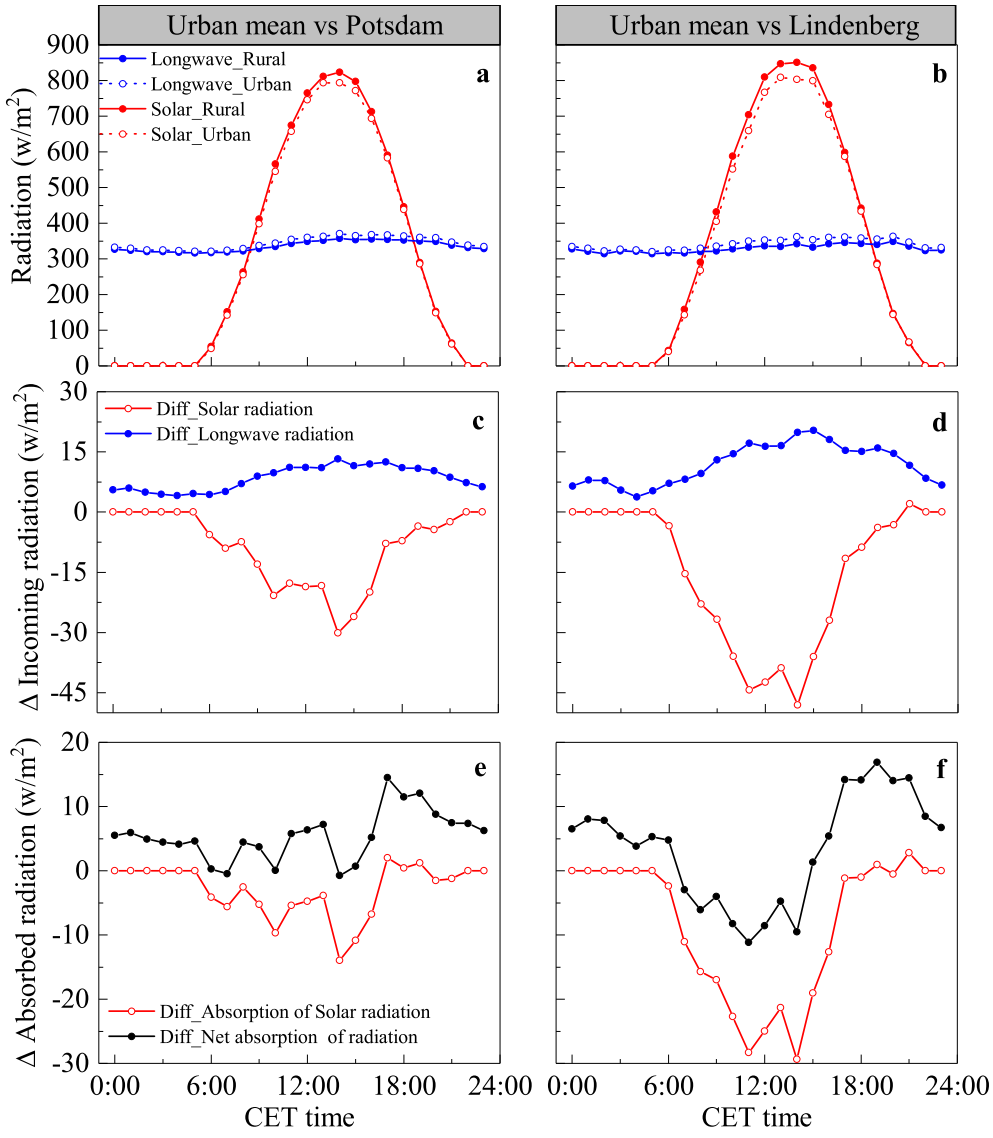

Fig. 6. Diurnal variations of the mean incoming solar radiation and atmospheric longwave radiation (upper panels a and b), and their urban-rural difference (middle panels c and d), and the urban-rural difference of the net absorption of radiation (lower panels e and f) in June, July, and August from 2010 to 2017. Subplots (a), (c) and (e) show the comparison between urban stations and Potsdam station, and subplots (b), (d), and (f) show the comparison between urban stations and Lindenberg station. The urban curves in subplot (a) and (b) are mean radiation observed at all urban stations in Table 1. The mean values at each hour were calculated under clear sky conditions with cloudy time omitted.

Boucher, 2000). On the one hand, aerosol particles scatter solar radiation back to the space, reducing the solar radiation reaching the surface (e.g. Jin et al., 2010). On the other hand, aerosol particles absorb infrared radiation emitted by the earth surface, especially within the longwave atmospheric window (wavelength range 8–12 mm) (e.g. Lubin and Simpson, 1994; Vogelmann et al., 2003), and some aerosol particles, such as black carbon, absorb solar radiation (e.g. Gatari and Boman, 2003; Ramanathan and Carmichael, 2008), heating the atmosphere. The heated atmosphere re-emits more longwave radiation to the surface. The dense aerosols in the urban atmosphere can reduce more solar radiation and increase more atmospheric longwave radiation, compared to the thin aerosols in rural areas. Additionally, the warmer urban surface could emit larger upward longwave radiation, promoting the heating of the atmosphere through the absorption of the aerosols and the following re-emission of the longwave radiation (Oke, 1982). As a result, urban areas receive less solar radiation and more atmospheric longwave radiation, as shown in Fig. 6. The similar phenomena were also reported by other studies. Estournel et al. (1983) found that the urban site received 30 W/m^2 less solar radiation and 15 to 25 W/m^2 more longwave radiation than the rural site during cloudless days in Toulouse. Jauregui and Luyando (1999) reported that on average the Mexico City received 21.6% less solar energy than the rural surroundings on clear days during the dry season. Robaa (2009) found that the attenuation of solar radiation in the urban area was always higher than that in rural area in Greater Cairo region, and the urban-rural difference of the attenuation increased in the past years, because urbanization and industrialization processes produced more pollutants. Wang et al. (2015) reported that the monthly-averaged incoming solar radiation and longwave radiation at urban site was 3–20% lower and 3–15% higher than those at rural site in Beijing.

Urban surface allocates more heat to the atmosphere than natural surface, leading to the warmer atmosphere in urban areas than in rural areas (Oke, 1982). The UHI-related warm urban atmosphere may also strengthen the emission of atmospheric longwave radiation. Our observation data did not exclude this factor. However, UHI effect mainly exists within a thin layer near the ground and decreases fast with the increase of height due to the advection by strong wind in high-altitude (Chao, 1991). Rouse et al. (1973) and Tapper (1990) reported that the urban-rural difference of the mean atmosphere temperature of the boundary layer did not differ significantly. The urban-rural difference

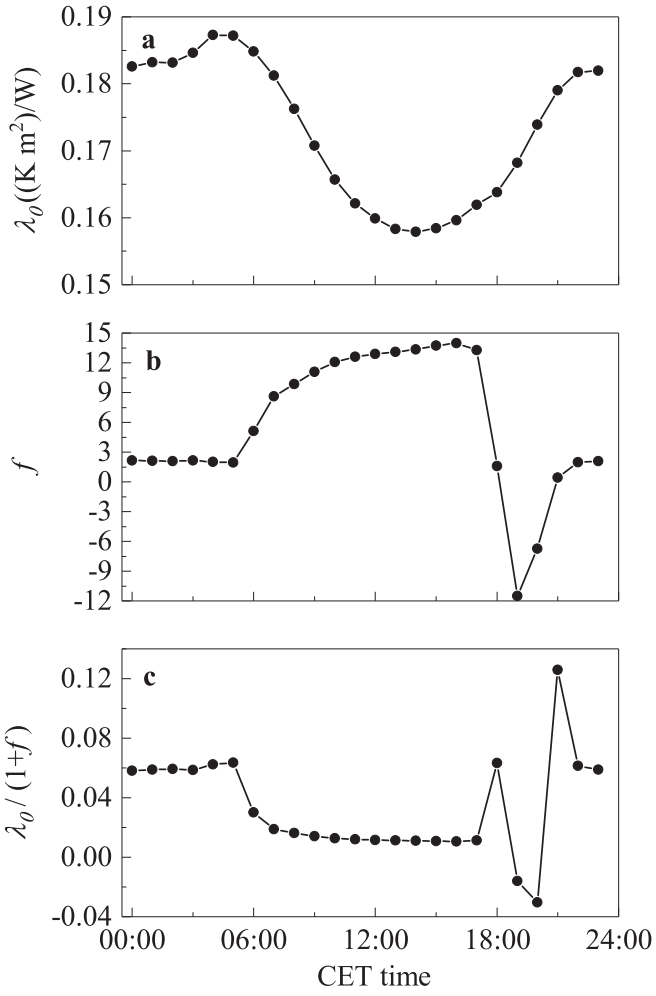

Fig. 7. Diurnal variations of the (a) λ_0, (b) f, and $\lambda_0/(1+f)$ in summer.

of the longwave radiation emission caused by the difference of the atmospheric temperature in the boundary layer was small. In our study, the urban-rural difference of the incoming longwave radiation did not increase with the increase of AUHII (Fig. S5). The larger urban-rural difference of the incoming longwave radiation appeared during the day, when the city had more loading aerosols, not at night, when the AUHI was strong (Fig. 6). The impact of the UHI-related warm atmosphere

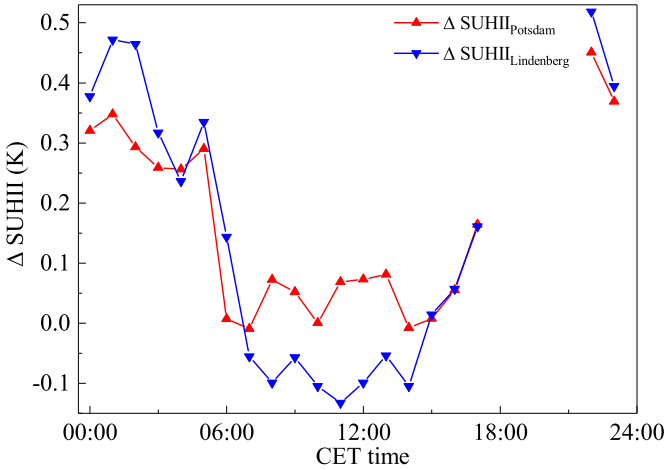

Fig. 8. Diurnal variation of the ΔSUHII in summer.

Table 2
The ΔSUHII caused by the urban-rural difference of net absorption of radiation in different time periods (mean ± Standard_deviation, K).

Time	$\Delta SUHII_{Potsdam}$	$\Delta SUHII_{Lindenberg}$
Day	0.06 ± 0.07	−0.00 ± 0.13
Night	0.33 ± 0.09	0.40 ± 0.09

on the increase of the incoming longwave radiation in the urban areas may be rather limited.

This study only revealed the direct effect of aerosols on radiation transfer and its following effect on SUHI. The radiation data were filtered with the cloudless condition. Nevertheless, aerosols also can affect radiation transfer processes indirectly, by affecting the formation and development of clouds (Mahowald, 2011). The indirect effect of aerosols is more complicated than its direct effect and has some uncertainties (Lohmann and Feichter, 2005). The indirect radiative effect of aerosols on UHI needs further study. Additionally, some gaseous pollut.

4.3. The influence of urban-rural difference of incoming radiation on SUHI

The influence of the urban-rural difference of incoming radiation on SUHI is affected by the surface albedo and sensitivity of the surface to the change of absorbed radiation (Oke, 1982). During the day, the urban-rural difference of incoming solar radiation is usually larger than the urban-rural difference of incoming longwave radiation (e.g. Estournel et al., 1983; Wang et al., 2015). Our results also show this phenomenon (Fig. 6b and c). However, as the albedo of the urban surface is lower than that of the natural surface, the urban-rural difference of absorbed solar radiation is reduced (Fig. 6e and f). Then the offset of the absorbed solar radiation and longwave radiation makes the urban-rural difference of net radiation absorption rather small (Oke, 1982). Moreover, the sensitivity of the surface temperature to the change of absorbed radiation is weak during the day (Fig. 7). Thus, the change of daytime SUHI caused by the urban-rural difference of absorbed energy is rather limited. At night, only longwave radiative forcing exists and the urban areas absorb more energy. Furthermore, the nighttime energy redistribution factor is small, resulting in the strong response of the surface to the change of absorbed radiation. As a result, the nighttime SUHI is enhanced by the more absorbed radiation in urban areas, as also found in Chinese cities (e.g. Cao et al., 2016).

It should be noted that the values of the ΔSUHII in Fig. 8 were only calculated for summer. In winter, the urban-rural difference of the incoming radiation may be very small because of the decrease of the magnitude of the radiation (Wang et al., 2015), in spite of the increase of urban aerosols. Nevertheless, the surface sensitivity to the change of radiation in winter is larger than that in summer (Bright et al., 2017). The winter ΔSUHII caused by the urban-rural difference of radiation needs further study.

5. Conclusions

This study aimed to enhance the understanding of the interactive influence between UHI and UPI during summer in the city of Berlin through a combined analysis of in-situ and remote sensing observations of aerosols and meteorological variables from 2010 to 2017. The study area showed both SUHI and AUPI. There was a positive correlation between the spatial configurations of the SUHI and AUPI, with a coefficient of 0.62 ($p < 0.01$) during the day. UHI-related warm temperature promoted the turbulent dispersion of aerosol particles in the urban areas, decreasing the NSUPI. The NSUPI intensity showed a negative relationship with the AUHI intensity, especially at night. The increased aerosols in the urban areas reduced the incoming solar radiation and increased the atmospheric longwave radiation. The SUHI was more sensitive to the change of absorbed radiation at night than during the day. It was estimated that the SUHI was enhanced by around 12% by the increased

absorbed radiation in the urban areas at clear night using an attribution method. During the day, the change of SUHI intensity caused by the change of the incoming radiation was negligible, due to the offset of the opposite change of solar radiation and atmospheric longwave radiation and the weak sensitivity of the surface.

Our results imply that the mitigation of UPI could decrease the urban-rural difference of the incoming radiation, contributing to the mitigation of UHI at night, while the mitigation of UHI may have a negative impact on the near-surface pollution concentrations. Additional, the reduction of pollutant emissions promotes the reduction of anthropogenic heat emission, which is a contribution to UHI (Taha, 1997). Decreasing the emissions of aerosol pollutants should be given priority for the improvement of urban thermal environment and air quality. On the contrary, designing mitigation strategies of UHI should be carefully treated and considers the consequent change of air quality. Strategies that are better for both urban thermal environment and air quality are preferable. Our study shows some insights regarding the interaction between UHI and UPI that provide starting points for urban planning authorities in order to design reasonable mitigation strategies. This study mainly focuses on the overall characteristics of the UHI and UPI and their interaction in a city scale. Other factors that may affect the UHI and UPI, such as urban texture, vegetation, and water bodies, are not considered and need further studies in the future. The effects of these potential mitigation strategies of UHI and UPI need further evaluations using numerical modelling and other methods before practical application.

Acknowledgments

This research is supported by the China Scholarship Council. Authors would like to thank Dr. Ines Langer from Freie Universität Berlin for the radiation data at FUB station and the air temperature data at Fasanenstrasse station. Thanks Ralf Becker, Lionel Doppler, and the group radiation processes (MOL4) of the observatory DWD/MOL-RAO (Deutscher Wetterdienst/Meteorologisches Observatorium Lindenberg–Richard Assmann Observatorium) for the radiation data at Tegel station. Thanks Dr. Andreas Kerschbaumer from Berlin Senate for the PM10 data. Thanks Daniel Fenner from Technische Universität Berlin for the discussion of results and the preparation of radiation data from the UCON (Urban Climate Observation network) stations TUB and Wienerstrasse. This study contributes to the research programme 'Urban Climate Under Change ([UC]²)', funded by the German Ministry of Research and Education (FKZ 01LP1602A). Special thanks go to Patricia Margerison for proofreading this manuscript.

Appendix A. Supplementary data

Supplementary data to this article can be found online at https://doi.org/10.1016/j.scitotenv.2018.04.254.

References

American Association for the Advancement of Science (AAAS), 2016. Rise of the city. Science 352, 906–907.

Baklanov, A., Lawrence, M., Pandis, S., Mahura, A., Finardi, S., Moussiopoulos, N., Beekmann, M., Laj, P., Gomes, L., Jaffrezo, J.L., Borbon, A., Coll, I., Gros, V., Sciare, J., Kukkonen, J., Galmarini, S., Giorgi, F., Grimmond, S., Esau, I., Stohl, A., Denby, B., Wagner, T., Butler, T., Baltensperger, U., Builtjes, P., Hout, D., Gon, H.D., Collins, B., Schluenzen, H., Kulmala, M., Zilitinkevich, S., Sokhi, R., Friedrich, R., Theloke, J., Kummer, U., Jalkinen, L., Halenka, T., Wiedensholer, A., Pyle, J., Rossow, W.B., 2010. MEGAPOLI: concept of multi-scale modeling of megacity impact on air quality and climate. Adv. Sci. Res. 4, 115–120.

Baklanov, A., Molina, L.T., Gauss, M., 2016. Megacities, air quality and climate. Atmos. Environ. 126, 235–249.

Bonn, B., Schneidemesser, E., Andrich, D., Quedenau, J., Gerwig, H., Lüdecke, A., Kura, J., Pietsch, A., Ehlers, C., Klemp, D., Kofahl, C., Nothard, R., Kerschbaumer, A., Junkermann, W., Grote, R., Pohl, T., Weber, K., Lode, B., Schönberger, P., Churkina, G., Butler, T.M., Lawrence, M.G., 2016. BAERLIN2014–the influence of land surface types on and the horizontal heterogeneity of air pollutant levels in Berlin. Atmos. Chem. Phys. 16, 7785–7811.

Bright, R.M., Davin, E., O'Halloran, T., Pongratz, J., Zhao, K., Cescatti, A., 2017. Local temperature response to land cover and management change driven by non-radiative processes. Nat. Clim. Chang. 7 (4), 296–302.

Burkart, K., Canário, P., Breitner, S., Schneider, A., Scherber, K., Andrade, H., Alcoforado, M.J., Endlicher, W., 2013. Interactive short-term effects of equivalent temperature and air pollution on human mortality in Berlin and Lisbon. Environ. Pollut. 183, 54–63.

Cao, C., Lee, X., Liu, S., Schultz, N., Xiao, W., Zhang, M., Zhao, L., 2016. Urban heat islands in China enhanced by haze pollution. Nat. Commun. 7. https://doi.org/10.1038/ncomms12509.

Chakraborty, T., Sarangi, C., Tripathi, S.N., 2017. Understanding diurnality and inter-seasonality of a sub-tropical urban heat island. Bound.-Layer Meteorol. 163 (2), 287–309.

Chao, Z., 1991. Urban climate and air pollution in Shanghai. Energ. Buildings 16 (1), 647–656.

Crutzen, P., 2004. New directions: the growing urban heat and pollution island effect-impact on chemistry and climate. Atmos. Environ. 38 (21), 3539–3540.

Dupont, E., Menut, L., Carissimo, B., Pelon, J., Flamant, P., 1999. Comparison between the atmospheric boundary layer in Paris and its rural suburbs during the ECLAP experiment. Atmos. Environ. 33 (6), 979–994.

Epstein, S.A., Lee, S.M., Katzenstein, A.S., Carreras-Sospedra, M., Zhang, X., Farina, S.C., Vahmani, P., Fine, P.M., Ban-Weiss, G., 2017. Air-quality implications of widespread adoption of cool roofs on ozone and particulate matter in southern California. Proc. Natl. Acad. Sci. 114 (34), 8991–8996.

Estournel, C., Vehil, R., Guedalia, D., Fontan, J., Druilhet, A., 1983. Observations and modeling of downward radiative fluxes (solar and infrared) in urban/rural areas. J. Clim. Appl. Meteorol. 22 (1), 134–142.

Fallmann, J., 2014. Numerical Simulations to Assess the Effect of Urban Heat Island Mitigation Strategies on Regional Air Quality. Universität zu Köln http://kups.ub.uni-koeln.de/5913/.

Fallmann, J., Forkel, R., Emeis, S., 2016. Secondary effects of urban heat island mitigation measures on air quality. Atmos. Environ. 125, 199–211.

Fenner, D., Meier, F., Scherer, D., Polze, A., 2014. Spatial and temporal air temperature variability in Berlin, Germany, during the years 2001–2010. Urban Climate 10, 308–331.

Feranec, J., Hazeu, G., Christensen, S., Jaffrain, G., 2007. Corine land cover change detection in Europe (case studies of the Netherlands and Slovakia). Land Use Policy 24 (1), 234–247.

Gabriel, K.M., Endlicher, W.R., 2011. Urban and rural mortality rates during heat waves in Berlin and Brandenburg, Germany. Environ. Pollut. 159 (8), 2044–2050.

Gatari, M.J., Boman, J., 2003. Black carbon and total carbon measurements at urban and rural sites in Kenya, East Africa. Atmos. Environ. 37 (8), 1149–1154.

Gedzelman, S.D., Austin, S., Cermak, R., Stefano, N., Partridge, S., Quesenberry, S., Robinson, D.A., 2003. Mesoscale aspects of the urban heat island around New York City. Theor. Appl. Climatol. 75 (1), 29–42.

Gelaro, R., McCarty, W., Suárez, M.J., Todling, R., Molod, A., Takacs, L., Randles, C.A., Darmenova, A., Bosilovicha, A.G., Reichlea, R., Wargan, K., Coy, L., Cullather, R., Draper, C., Akella, S., Buchard, V., Conaty, A., Silva, A.M., Gu, W., Kim, G., Koster, R., Lucchesi, R., Merkova, D., Nielsen, J.E., Partyka, G., Pawson, S., Putman, W., Rienecker, M., Schubert, S.D., Sienkiewicz, M., Zhao, B., 2017. The modern-era retrospective analysis for research and applications, version 2 (MERRA-2). J. Clim. 30 (14), 5419–5454.

Godowitch, J.M., Ching, J.K.S., Clarke, J.F., 1985. Evolution of the nocturnal inversion layer at an urban and nonurban location. J. Clim. Appl. Meteorol. 24 (8), 791–804.

Görgen, R., Lambrecht, U., 2007. Particulate matter in ambient air. J. Eur. Environ. Plann. Law 4, 278–288.

Han, X., Naeher, L.P., 2006. A review of traffic-related air pollution exposure assessment studies in the developing world. Environ. Int. 32 (1), 106–120.

Haywood, J., Boucher, O., 2000. Estimates of the direct and indirect radiative forcing due to tropospheric aerosols: a review. Rev. Geophys. 38 (4), 513–543.

Jauregui, E., Luyando, E., 1999. Global radiation attenuation by air pollution and its effects on the thermal climate in Mexico City. Int. J. Climatol. 19 (6), 683–694.

Jin, M., Shepherd, J.M., Zheng, W., 2010. Urban surface temperature reduction via the urban aerosol direct effect: a remote sensing and WRF model sensitivity study. Adv. Meteorol. https://doi.org/10.1155/2010/681587.

Kuik, F., Lauer, A., Churkina, G., Gon, H.A.D., Fenner, D., Mar, K.A., Butler, T.M., 2016. Air quality modelling in the Berlin-Brandenburg region using WRF-Chem v3.7.1: sensitivity to resolution of model grid and input data. Geosci. Model Dev. 9 (12), 4339.

Lai, L.W., Cheng, W.L., 2010. Urban heat island and air pollution-an emerging role for hospital respiratory admissions in an urban area. J. Environ. Health 72 (6), 32–35.

Lee, X., Goulden, M.L., Hollinger, D.Y., Barr, A., Black, T.A., Bohrer, G., Bracho, R., Drake, B., Goldstein, A., Gu, L., Katul, G., Kolb, T., Law, B.E., Margolis, H., Meyers, T., Monson, R., Munger, W., Oren, R., Paw, U.K.T., Richardson, A.D., Schmid, H.P., Staebler, R., Wofsy, S., Zhao, L., 2011. Observed increase in local cooling effect of deforestation at higher latitudes. Nature 479, 384–387.

Lee, X., Gao, Z., Zhang, C., Chen, F., Hu, Y., Jiang, W., Liu, S., Lu, L., Sun, J., Wang, J., Zeng, Z., Zhang, Q., Zhao, M., Zhou, M., 2015. Priorities for boundary layer meteorology research in China. Bull. Am. Meteorol. Soc. 96 (9), 149–151.

Li, H., Wolter, M., Wang, X., Sodoudi, S., 2017. Impact of land cover data on the simulation of urban heat island for Berlin using WRF coupled with bulk approach of Noah-LSM. Theor. Appl. Climatol. https://doi.org/10.1007/s00704-017-2253-z.

Li, H., Zhou, Y., Li, X., Meng, L., Wang, X., Wu, S., Sodoudi, S., 2018. A new method to quantify surface urban heat island intensity. Sci. Total Environ. 624, 262–272.

Lohmann, U., Feichter, J., 2005. Global indirect aerosol effects: a review. Atmos. Chem. Phys. 5 (3), 715–737.

Lubin, D., Simpson, A.S., 1994. The longwave emission signature of urban pollution: radiometric FTIR measurement. Geophys. Res. Lett. 21 (1), 37–40.

Lutz, M., 2013. Mitigation strategies: Berlin, Germany. Particulate Matter: Environmental Monitoring and Mitigation:pp. 74–95 https://doi.org/10.4155/ebo.13.489.
Mahowald, N., 2011. Aerosol indirect effect on biogeochemical cycles and climate. Science 334, 794–796.
McDonnell, M.J., MacGregor-Fors, I., 2016. The ecological future of cities. Science (6288), 936–938.
Meng, X., Zhang, Y., Zhao, Z., Duan, X., Xu, X., Kan, H., 2012. Temperature modifies the acute effect of particulate air pollution on mortality in eight Chinese cities. Sci. Total Environ. 435, 215–221.
Monn, C., Becker, S., 1999. Cytotoxicity and induction of proinflammatory cytokines from human monocytes exposed to fine (PM2. 5) and coarse particles (PM10–2.5) in outdoor and indoor air. Toxicol. Appl. Pharmacol. 155 (3), 245–252.
Munchak, L.A., Levy, R.C., Mattoo, S., Remer, L.A., Holben, B.N., Schafer, J.S., Hostetler, C.A., Ferrare, R.A., 2013. MODIS 3 km aerosol product: applications over land in an urban/suburban region. Atmos. Meas. Tech. 6, 1747–1759.
Ohara, T., Akimoto, H., Kurokawa, J.I., Horii, N., Yamaji, K., Yan, X., Hayasaka, T., 2007. An Asian emission inventory of anthropogenic emission sources for the period 198–2020. Atmos. Chem. Phys. 7 (16), 4419–4444.
Oke, T.R., 1982. The energetic basis of the urban heat island. Q. J. R. Meteorol. Soc. 108 (455), 1–24.
Oke, T.R., 1995. The Heat Island of the Urban Boundary Layer: Characteristics, Causes and Effects. Wind Climate in Cities. Springer, Dordrecht, pp. 81–107.
Ramanathan, V., Carmichael, G., 2008. Global and regional climate changes due to black carbon. Nat. Geosci. 1 (4), 221.
Remer, L.A., Mattoo, S., Levy, R.C., Munchak, L.A., 2013. MODIS 3 km aerosol product: algorithm and global perspective. Atmos. Meas. Tech. 6 (7), 1829.
Rendón, A.M., Salazar, J.F., Palacio, C.A., Wirth, V., Brötz, Björn, 2014. Effects of urbanization on the temperature inversion breakup in a mountain valley with implications for air quality. J. Appl. Meteorol. Climatol. 53 (4), 840–858.
Rizwan, A.M., Dennis, L.Y.C., Liu, C., 2008. A review on the generation, determination and mitigation of Urban Heat Island. J. Ecol. Environ. Sci. 20, 120–128.
Robaa, S.M., 2009. Urban–rural solar radiation loss in the atmosphere of Greater Cairo region, Egypt. Energy Convers. Manag. 50 (1), 194–202.
Rouse, W.R., Noad, D., McCutcheon, J., 1973. Radiation, temperature and atmospheric emissivities in a polluted urban atmosphere at Hamilton, Ontario. J. Appl. Meteorol. 12 (5), 798–807.
Sarrat, C., Lemonsu, A., Masson, V., Guedaliac, D., 2006. Impact of urban heat island on regional atmospheric pollution. Atmos. Environ. 40 (10), 1743–1758.
Schaaf, C.B., Gao, F., Strahler, A.H., Lucht, W., Li, X., Tsang, T., Strugnell, N.C., Zhang, X., Jin, Y., Muller, J.P., Lewis, P., Barnsley, M., Hobson, P., Disney, M., Roberts, G., Dunderdale, M., Doll, C., Entremont, R.P., Hu, B., Liang, S., Privette, J.L., Roy, D., 2002. First operational BRDF, albedo nadir reflectance products from MODIS. Remote Sens. Environ. 83 (1), 135–148.
Scherer, D., Fehrenbach, U., Lakes, T., Lauf, S., Meier, F., Schuster, C., 2014. Quantification of heat-stress related mortality hazard, vulnerability and risk in Berlin, Germany. DIE ERDE–J. Geogr. Soc. Berlin 144, 238–259.
Schwarz, N., Lautenbach, S., Seppelt, R., 2011. Exploring indicators for quantifying surface urban heat islands of European cities with MODIS land surface temperatures. Remote Sens. Environ. 115 (12), 3175–3186.
Shahraiyni, H.T., Sodoudi, S., Kerschbaumer, A., Cubasch, U., 2015. The development of a dense urban air pollution monitoring network. Atmos. Pollut. Res. 6 (5), 904–915.
Sokhi, R.S., Baklanov, A., Piringer, M., 2017. Special issue of journal of urban climate: modelling of urban air pollution and climate interactions. Urban climate 22:1. https://doi.org/10.1016/j.uclim.2017.11.002.
Taha, H., 1997. Urban climates and heat islands: albedo, evapotranspiration, and anthropogenic heat. Energ. Buildings 25 (2), 99–103.
Tapper, N.J., 1990. Urban influences on boundary layer temperature and humidity: results from Christchurch, New Zealand. Atmos. Environ. 24 (1), 19–27.
Vogelmann, A.M., Flatau, P.J., Szczodrak, M., Markowicz, K.M., Minnett, P.J., 2003. Observations of large aerosol infrared forcing at the surface. Geophys. Res. Lett. 30 (12). https://doi.org/10.1029/2002GL016829.
Wagner, P., Schäfer, K., 2017. Influence of mixing layer height on air pollutant concentrations in an urban street canyon. Urban Climate 22, 64–79.
Wan, Z., 2008. New refinements and validation of the MODIS land-surface temperature/emissivity products. Remote Sens. Environ. 112 (1), 59–74.
Wan, Z., 2014. New refinements and validation of the collection-6 MODIS land-surface temperature/emissivity product. Remote Sens. Environ. 140, 36–45.
Wan, Z., Dozier, J., 1996. A generalized split-window algorithm for retrieving land-surface temperature from space. IEEE Trans. Geosci. Remote Sens. 34 (4), 892–905.
Wang, L., Gao, Z., Miao, S., Guo, X., Sun, T., Liu, M., Li, D., 2015. Contrasting characteristics of the surface energy balance between the urban and rural areas of Beijing. Adv. Atmos. Sci. 32 (4), 505.
Wei, Y.D., Ye, X., 2014. Urbanization, urban land expansion and environmental change in China. Stoch. Env. Res. Risk A. 28 (4), 757–765.
Xu, L.Y., Xie, X.D., Li, S., 2013. Correlation analysis of the urban heat island effect and the spatial and temporal distribution of atmospheric particulates using TM images in Beijing. Environ. Pollut. 178, 102–114.
Zhao, L., Lee, X., Smith, R.B., Oleson, K., 2014. Strong contributions of local background climate to urban heat islands. Nature 511, 216–219.